Ultrawide-Bandgap Semiconductors for High-Frequency Devices

Spyridon Pavlidiso, Greg Medwigo, and Michael Thomas

ellular base stations for 5G/6G networks, as well as satellites and long-range radar for commercial, aerospace, and defense systems all demand power amplifiers (PAs) with high output power density and high efficiency. While silicon (Si), silicon germanium (SiGe), and gallium arsenide (GaAs) technologies are well established, it is now impossible to overlook gallium nitride (GaN) in applications where maximizing output power with minimal footprint is paramount. Backed by its deployment for solid-state lighting, power converters, and PAs, GaN technology has seen tremendous advancements in the last 20-30 years. The principal device for



Spyridon Pavlidis (spavlidis@ncsu.edu) and Greg Medwig (gmedwig@ncsu.edu) are with the Department of Electrical and Computer Engineering, North Carolina State University, Raleigh, NC 27606 USA. Michael Thomas (mwthoma4@ncsu.edu) is with the Department of Materials Science and Engineering, North Carolina State University, Raleigh NC 27606, USA.

> Digital Object Identifier 10.1109/MMM.2024.3428193 Date of current version: 18 September 2024

microwave and millimeter-wave (mm-wave) applications is the AlGaN/GaN high-electron-mobility transistor (HEMT), which is most commonly fabricated on either silicon carbide (SiC) or Si substrates. AlGaN/GaN HEMTs with an output power density of 40 W/mm [1] have been reported up to the X band, while highly scaled transistors with $f_t/f_{\rm MAX}$ of >450 GHz have also been achieved [2]. In the last decade, a new wave of innovations has also emerged, such as the replacement of AlGaN barriers with scandium aluminum nitride (ScAlN) and the development of N-polar GaN technology with 8-W/mm power density at 94 GHz [3].

Fundamentally, these achievements are driven by GaN's properties as a wide-bandgap (WBG) semiconductor, which allow it to sustain high electric fields and operate at high temperatures, simplifying system cooling requirements and facilitating deployment in extreme environments. The success of the "WBG revolution," in part driven by GaN's popularity, has prompted significant private and public investment in GaN HEMT technology. To maintain competitive superiority, an important question is now looming: "Is there a technology capable of outperforming GaN?" The answer may be found in ultrawide-bandgap (UWBG) semiconductors, notably gallium oxide (Ga₂O₃), Al-rich compositions of aluminum gallium nitride (Al_xGa_{1-x}N), aluminum nitride (AlN), diamond, and cubic boron nitride (c-BN). UWBG semiconductors (UWBGSs) are benefiting from accelerated advances in substrate quality and availability, epitaxy, and fabrication process technologies, leading to initial high-frequency device demonstrations. Thus, the objective of this article is to review the current status of UWBGSs as candidates for the next generation of microwave and mm-wave PAs.

What Makes AlGaN/GaN HEMTs Attractive for Microwave PAs?

To assess the prospects of UWBGS transistors for high-power amplifiers, it is important to first appreciate what characteristics have permitted AlGaN/GaN HEMTs to surpass incumbent technologies and what challenges limit performance. A cross-sectional schematic of a typical AlGaN/GaN HEMT is provided in Figure 1. The conducting channel is located on the GaN side of the AlGaN/GaN heterojunction within a quantum well or 2D electron gas (2DEG). Unlike modulation-doped field-effect transistors (MOD-FETs) realized in conventional III-V technology, spontaneous and piezoelectric polarization effects permit channel formation without impurity doping in the III-nitride layers. The gate, typically a T-gate to enable high-frequency performance with short gate length (L_G), is a Schottky contact that can optionally involve barrier recess etching or gate insulator deposition prior to metal deposition. The device's speed is captured by the transit delay time (τ_T) , or the time it takes an electron to traverse the channel, which is dependent on the applied electric field and the electron's velocity.

By adopting the assumptions that L_G represents the entire channel and that the semiconductor is pushed to its critical electric field (E_C) where electrons experience

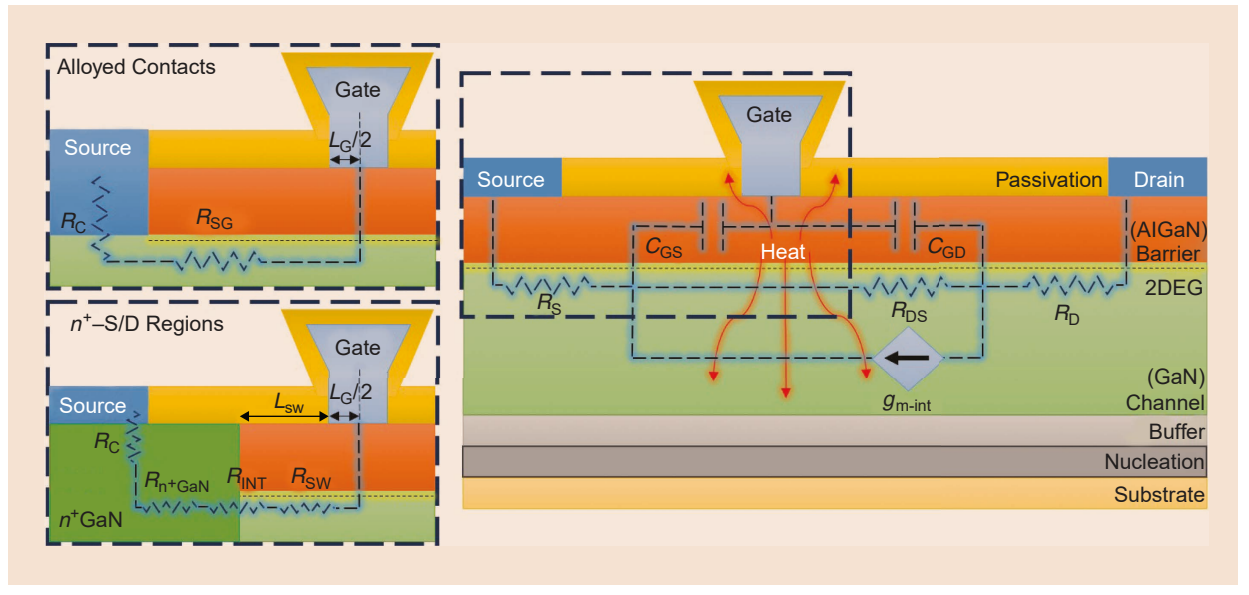


Figure 1. A cross section and an equivalent circuit model of an HEMT. Specific materials are provided by way of example for an AlGaN/GaN HEMT. Two different ohmic contact schemes can be used to form the source and drain regions, namely, alloyed contacts or etch-and-regrown contacts. 2DEG: 2D electron gas.

velocity saturation (ν_s), the Johnson figure of merit (JFOM) can be defined to compare semiconductor materials in high-frequency transistors:

$$JFOM = f_T V_{BR} = \frac{E_C \nu_s}{2\pi}$$
 (1)

where f_T is the transit frequency, and V_{BR} is the device's breakdown voltage. When one compares GaN to GaAs in terms of E_C (3.4 MV/cm versus 0.4 MV/cm) and ν_s (2.4 × 10^7 cm/s versus 0.9 × 10^7 cm/s), the allure of a GaN channel is quickly appreciated. Of course, the picture is not so simplistic in practice, and a variety of parasitic effects have had to be addressed over the years.

First, source access resistance (R_s) and drain access resistance (R_D) must be considered because they contribute to increased ohmic losses and increased charging delays linked to the parasitic contact resistance (R_C) elements depicted in Figure 1. The most common method for ohmic contact formation is through alloying, typically achieved by the rapid thermal annealing (RTA) of Ti/Al/Ni/Au contacts deposited on top of the AlGaN barrier. As shown in Figure 1, R_S is, thus, the sum of R_C and the source-togate channel resistance (R_{SG}). In GaN, R_C is typically $0.3-0.5 \Omega$ ·mm, which is significant compared to what is achievable in state-of-the-art GaAs or InP technologies. R_{SG} is proportional to the sheet resistance (R_{SH}) and the source-to-gate distance (L_{SG}) . Typical channel mobilities (μ) and sheet charge densities (N_S) are ~1,500 cm²/Vs and ~10¹³ cm⁻², respectively, corresponding to sheet resistances of ~400 Ω/\Box .

To reduce R_S , highly doped (n⁺-GaN) access regions can be introduced by ion implantation of Si or etch and regrowth. The latter is now the preferred approach because contacts can be deposited directly onto n⁺⁺-GaN, and the thermal budget is more favorable, which is both compatible with self-aligned gate processes and does not deteriorate channel mobility due to the need for high temperature annealing. In this implementation, R_C can be reduced to 0.03Ω ·mm, while the regrown region has a sheet resistance of 40– 50Ω / \square . These achievements demonstrate the importance of efficient doping to push the limits of performance.

Surface engineering represents another key area for AlGaN/GaN HEMTs. For example, the passivation of surface states is required to reduce drain lag, which impacts output power and efficiency at high frequency. The most common solution is plasmaenhanced chemical vapor deposition (PECVD) silicon nitride (SiN). To reduce surface leakage current, the bandgap of the dielectric passivation material must be sufficiently large compared to the semiconductor, a requirement that becomes challenging when UWBGSs are considered. The JFOM assumes that electrons pass through the channel at a constant ν_s

while experiencing a constant field. In reality, the field varies across the channel, with the peak located on the drain side of the gate electrode. The reduction of L_{SG} and use of highly doped source access structures (Figure 1) can reduce the source-side electric field and improve transconductance [4], [5]. However, L_{GD} is directly proportional to breakdown voltage and cannot be reduced without consequence. Field plate structures are thus needed, but these introduce parasitic capacitances that make them impractical at mm-waves and beyond.

Recently, the use of very-high-permittivity (k) dielectrics has also been proposed to increase the breakdown field [6]. It is additionally well documented that thermal dissipation plays a major role in limiting output power densities. The superior bulk thermal conductivity of SiC makes it a more attractive substrate than, for example, sapphire. Moreover, efforts are underway to "wrap" AlGaN/GaN HEMTs in diamond, with polycrystalline diamond deposited on the top surface and wafer bonding used to transfer devices to bulk diamond substrates. Nonetheless, it is now widely understood that significant thermal boundary resistance introduced by heterogeneous nucleation, as well as buffer and interface layers, remains a bottleneck [7]. Ideally, homoepitaxy can be used to form devices on low-cost, large-area substrates with high thermal conductivity and high electrical resistivity.

UWBGS Property Overview

From this discussion, it should be clear that not only must the intrinsic properties of the semiconductor be compelling to pursue its adoption in high-power, high-frequency transistors, but pathways toward an ecosystem of technologies that address parasitics must also exist. To assess this, Table 1 includes a comparison of many relevant material properties for the most popular UWBGSs. In addition to the JFOM, the Keyes FOM (KFOM) and Baliga FOM (BFOM) are introduced to further capture tradeoffs. The KFOM, which emphasizes thermal conductivity, is defined as

$$KFOM = \kappa_{th} \cdot \sqrt{\frac{c \cdot v_s}{4\pi\varepsilon_s}}$$
 (2)

where κ_{th} is bulk thermal conductivity, c is the speed of light, and ε_s is the semiconductor's dielectric permittivity. The BFOM, which is relevant to devices used in low-frequency power conversion applications, is defined as

$$BFOM = \varepsilon_s \mu E_C^3. \tag{3}$$

In addition to the electron mobility (μ_n), the hole mobility (μ_p) is also included in Table 1. While unipolar (n-channel) HEMTs are most established, μ_p is relevant to assessing the prospects of adopting UWBGSs in

bipolar devices, such as heterojunction bipolar transistors (HBTs). Generally, a large bandgap, high critical electric breakdown field, high carrier mobility and saturation velocity, low dielectric constant, and high thermal conductivity are desirable. Each material included herein has its own inherent strengths, weaknesses, and research limitations, which are discussed in the rest of this section.

With AlGaN/GaN HEMTs firmly established for high-power RF applications, it is natural to consider the transition to AlGaN and AlN technologies. By controlling the Al composition, the bandgap can be tuned between 3.4 eV (GaN) and 6 eV (AlN), which directly

correlates with the material's E_C and, therefore, its ability to produce high output power via voltage scaling. Since E_C increases with Al content, one might expect a monotonic increase in JFOM as a function of Al content. However, as shown in Figure 2, it is predicted that ν_s follows a "bathtub curve" relationship as a function of Al content, which means that the lowest JFOM value for $Al_xGa_{1-x}N$ -channel structures actually exists at x=0.23 [18]. It is important to note that the roll-off of μ_n as a function of Al content is even more aggressive than that for ν_s . This has important implications for access resistance in RF devices as well as for on resistance in power devices. AlN's high κ_{th} is also attractive

TABLE 1. The relevant material properties at room temperature.								
Property	Si	GaAs [10]	4H-SiC	GaN	β -Ga $_2$ O $_3$	Diamond	AIN	c-BN
E_g (eV)	1.12	1.42	3.23	3.4	4.9	5.5	6	6.4
Bandgap type	Indirect	Direct	Indirect	Direct	Direct	Indirect	Direct	Indirect
E_c (MV/cm)	0.3	0.4	2.8	3.5	10.3	13	15.4	17.5
$arepsilon_{ ext{r}}$ (static)	11.7	13.1	9.66	8.7	10	5.7	8.5	7.1 [11]
κ_{th} (W/cm*K)	1.45 [12]	0.55	3.7	2.5	0.1-0.3*	22.9 [12]	2.85	9.4 [12]
v _s (107 cm/s)	1.02 [13]	0.9	1.9	2.4	2 [14]	2.3	1.4	2.7 [15]
$\mu_{\rm n}$ (cm ² /Vs)	1,440	9,400 [16]	950	1,400	250	4,500	450	1,600 [15]
$\mu_{\rm p} \ ({\rm cm}^2/{\rm Vs}) \ [17]$	450	492 [16]	115	350	N/A	3,800	N/A	400 [15]
JFOM	1	1.38	302	754	2,734	9,548	4,964	23,843
BFOM	1	17	441	1,142	2,800	123,282	30,562	133,191
KFOM	1	0.3	3.83	3.07	0.31	33.98	2.7	13.54
Unless otherwise stated, data are from [8] or [9]. N/A: not available. *Anisotropic behavior: thermal conductivity in the [010] direction is higher than in the [100] direction [11].								

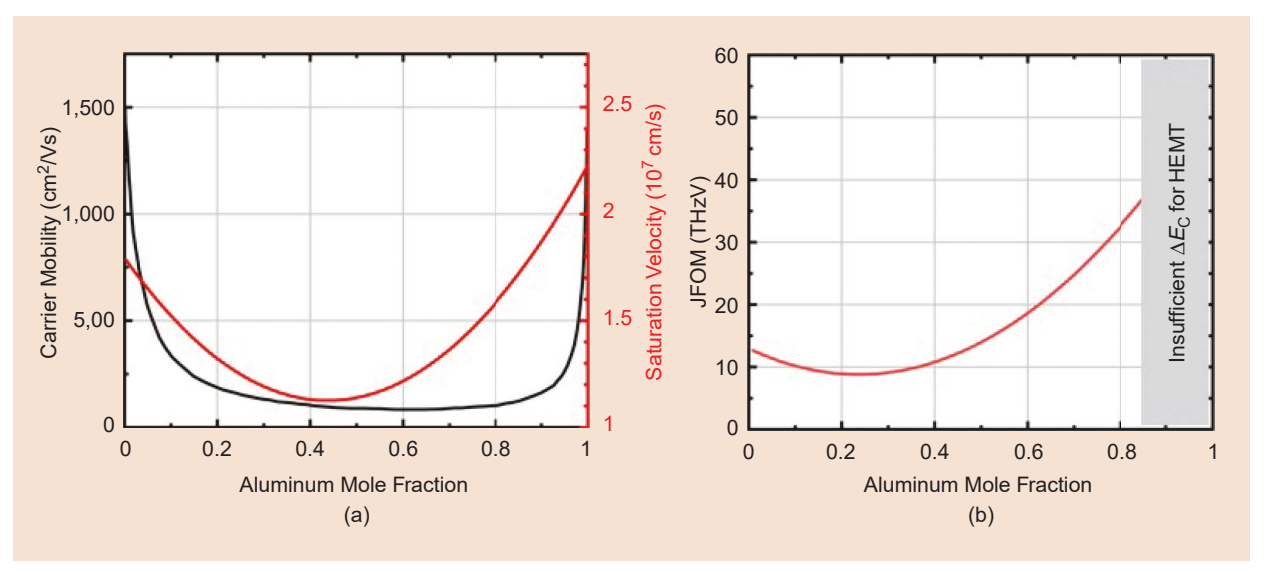


Figure 2. (a) The carrier mobility (at $N_S = 10^{13}$ cm⁻²) in a GaN/AlGaN heterostructure's 2DEG and the saturation velocity in AlGaN as functions of the aluminum content. (Source: adapted from [18]; used with permission.) (b) The JFOM as a function of Al content in AlGaN for HEMTs. Mole fractions (x) of x > 0.85 are excluded because the conduction band offset between a channel of that composition, and an AlN buffer layer would be insufficient to form a 2DEG. (Source: adapted from [18]; used with permission.)

for high-power applications, and it is electrically highly insulating, which minimizes parasitics at microwave and mm-wave frequencies.

Diamond has been the subject of great interest because it has comparatively large electron and hole mobilities, high saturation velocities for both carrier types, a high critical electric field, and the highest thermal conductivity of any known material. Having the highest thermal conductivity all but guarantees diamond's adoption in electronics as the backbone of future thermal management systems [7], [19]. It also results in diamond having the highest KFOM of all examined materials, more than an order of magnitude higher than GaN and AlN. Diamond's high critical electric field of 13 MV/cm, combined with very high electron mobility, also contributes to it having a very high BFOM, second only to that of c-BN and still more than 4× greater than that of AlN and 100× greater than that of GaN. In JFOM, diamond is still strong, at nearly 2× that of AlN and 3.5× that of β -Ga₂O₃, but it is less than half that of c-BN. Realizing those high electron and hole mobilities in devices has proven to be a significant challenge and remains a limiting factor between current diamond devices and their extremely high potential illustrated by the FOMs.

Gallium oxide is another strong contender for the next standard in RF electronics. It grows in many different phases, but the monoclinic beta phase (β -Ga₂O₃) is the most developed because of its stability. β -Ga₂O₃ can be grown with methods similar to those used for traditional Si boules. This compatibility with wellunderstood growth techniques like float zone, Czochralski, vertical Bridgman, and edge-defined film-fed growth means that high-quality, large (4-in) native substrates are readily available, despite the relative infancy of the material's interest as a semiconductor [20]. β -Ga₂O₃ performs well in FOMs, beating the existing WBG materials by 4–8× in JFOM and 2.5–7× in BFOM, though its FOMs are outstripped by the other UWBG materials discussed in this article. Its extremely low thermal conductivity of just 0.1-0.3 W/cm*K, depending on the direction, leads to an especially low KFOM. It is clear that high-power applications of β -Ga₂O₃ will also need strong thermal management setups implemented into their design at the device level.

c-BN is also rapidly gaining attention as a potential future candidate for RF applications. It has the second highest thermal conductivity of any known material, behind only diamond, and its small lattice mismatch with diamond (1.3%) may enable c-BN and diamond heterostructures [21] or may allow c-BN to be an effective interfacial layer between diamond and other materials like III-nitrides [8]. Both the critical electric field of c-BN and electron saturation velocity are expected to be the highest among the materials

discussed here, at 17.5 MV/cm and $2.7 \times 10^7 \text{ cm/s}$, respectively. These factors mean c-BN has, by far, the highest JFOM of all discussed material families, outperforming its nearest competitor (diamond) by a factor of $2.5 \times$ and GaN by nearly $32 \times$. Electron and hole mobilities similar to those observed in Si combine with the high critical electric field to also give c-BN a slight edge in BFOM over diamond. These factors, combined with its thermal conductivity being second behind only diamond, make c-BN a very interesting material to pursue.

The State of the Art for UWBGS-Based RF Devices

As noted, UWBGSs are currently available in varying degrees of maturity. This section aims to establish currently preferred device topologies and approaches for each material system, except for c-BN, with which devices have yet to be realized. Due to their relative simplicity and high speed, the focus is placed on lateral unipolar devices, such as metal–semiconductor field-effect transistors (MESFETs) and HEMTs.

UWBG III-Nitride Devices

Two device categories are considered in this technology space: those with UWBG AlGaN channels and hybrid devices in which WBG GaN channels are formed on UWBG AlN substrates and/or buffer layers. While the latter category does not strictly adhere to the definition of an UWBG device, it is worth discussing since initial reports hint at the potential to outperform conventional GaN-on-SiC HEMT technology.

In the first category, the exclusive use of UWBG III-nitrides has proven to be an effective pathway toward increasing breakdown fields ($E_{\rm B}$) in HEMTs. HEMTs with >50%-Al-content AlGaN channels on bulk AlN substrates have achieved an $E_{\rm B}$ of >11 MV/cm, but relatively large $R_{\rm SH}$ (>2,000 Ω/\square) and $R_{\rm C}$ (>4 Ω -mm) remain challenges [22], [23]. Due to cost constraints, however, most device demonstrations thus far have been on sapphire substrates. Approaches to ohmic contacts can be grouped into four categories: 1) conventional contact alloying, 2) molecular beam epitaxy (MBE)-based etch and regrowth, 3) a recessed channel using a single growth step with compositionally reverse-graded contact layers, and 4) constricted channel geometries.

Using the first strategy, $Al_{0.85}Ga_{0.15}N/Al_{0.7}Ga_{0.3}N$ HEMTs with L_G = 80 nm were fabricated, achieving f_T/f_{MAX} of 28.4/18.1 GHz and, at 3 GHz, P_{out} of 0.38 W/mm and power-added efficiency (PAE) of 11% [24]. Using the second strategy, $Al_{0.75}Ga_{0.25}N/Al_{0.6}Ga_{0.4}N$ HEMTs with L_G = 130 nm were fabricated, terminating the ohmic regions with GaN and resulting in an R_C of 7.5 Ω ·mm [25]. High-frequency testing resulted in f_T/f_{MAX} of 40/58 GHz and, at 10 GHz, P_{out} of 1.8 W/mm

and PAE of 22%. To reduce the contact resistance, the same authors adopted the third strategy and applied it to Al_{0.7}Ga_{0.3}N/Al_{0.5}Ga_{0.5}N, consequently achieving an $R_{\rm C}$ of 3.9 Ω ·mm [26]. They argued that exactly matching the exact Al composition of the AlGaN channel via etch and regrowth is difficult and explained that compositional mismatch at the regrown interface can introduce energy barriers that increase R_C . Using an L_G of 160 nm, f_T/f_{MAX} values of 20/40 GHz were achieved. The E_B of 2.8 MV/cm exceeds that of GaN-channel HEMTs.

Finally, constricted channel (or microchannel) devices have been used to reduce the impact of high $R_{\rm C}$ [Figure 3(a) and (b)], in turn enabling the majority of the applied V_{DS} to be dropped across the channel. Al_{0.65}Ga_{0.35}N/Al_{0.4}Ga_{0.6}N HEMTs with a microchannel width (W_{CH}) of 1 μ m and L_G of 100 nm achieved $I_{\text{MAX}} = 900 \text{ mA/mm}$; $f_{\text{T}}/f_{\text{MAX}}$ of 20/36 GHz; and, at 10 GHz, *P*_{out} of 2.7 W/mm [27] [Figure 3(c)]. It should be additionally noted that a variant of the AlGaN channel is the compositionally graded AlGaN channel [28], which may also provide linearity benefits.

Clearly, parasitic effects, such as low channel mobility and high contact resistance, still limit the output power of AlGaN-channel HEMTs, despite the record breakdown fields that have been reported in these devices. By fabricating devices with varying L_{G} , the effective saturation velocity in Al_{0.45}Ga_{0.55}N- and Al_{0.7}Ga_{0.3}N-channel HEMTs has been estimated to be 0.27×10^7 cm/s [29] and 0.38×10^7 cm/s [30], respectively. These values are lower than in GaN and lower than theory has predicted for AlGaN [31]. Nonetheless, if taken at face value, they indicate that a pathway toward high performance exists via voltage scaling, assuming parasitics can be eliminated. This argument is especially intriguing when combined with reports that the transport properties of AlGaN and AlN are less temperature sensitive than those of GaN [29], [32], which has motivated studies of high-temperature (>300 °C) studies of UWBG III-nitride HEMTs [33] and MESFETs [34].

The second approach is an evolution of current GaN HEMT technology, aiming to marry the benefits of GaN's high mobility in the channel with the large E_C of UWBG Al(Ga)N as the substrate and/or in the back barrier/buffer layers. Strictly speaking, this does not adhere to the definition of a UWBG device since GaN is employed as the channel. However, as is described, it appears that novel ways of integrating UWBG III-nitrides may improve performance compared to traditional designs. Thus, we have included them in this discussion.

Using thick AlN buffers layers grown on 6H-SiC substrates, AlN/GaN/AlN HEMTs with $N_s = 3 \times 10^{13}$ cm⁻², $\mu = 723 \text{ cm}^2/\text{Vs}$, and $R_{\text{SH}} = 293 \Omega/\Box$ [35]. By employing regrown n⁺-GaN contacts ($R_c = 0.15 \Omega \cdot mm$) and a highly scaled L_G of 50 nm, record f_T/f_{MAX} values of 123/233 GHz were achieved. Load-pull characterization at 10 GHz to identify input/output impedances at maximum PAE demonstrated gain (G_T) and P_{out} of 8.3 dB and 22 dBm (3 W/mm), respectively. In a separate publication, the authors reported an E_B of 1–2 MV/ cm with a maximum JFOM of 2.2 THz-V [36].

More recently, Al_{0.31}Ga_{0.69}N/GaN HEMTs on AlN substrates with carefully designed buffer layers have been reported [Figure 4(a)] with sheet resistance R_{SH} of $283 \Omega/\Box (N_s = 1.3 \times 10^{13} \text{ cm}^{-2}, \mu = 1,700 \text{ cm}^2/\text{Vs})$ and R_c of 0.1 Ω ·mm, with the latter once again enabled by regrown contacts [37]. Using L_G/L_{GD} of 250 nm/3 μ m, $f_T/$ f_{MAX} values of 24.1/52 GHz where achieved, along with a V_{BR} of 258 V (E_B < 1 MV/cm). This corresponds to a JFOM of 6.22 THz-V. Pulsed load pull with a 1% duty cycle (δ) at 8 GHz using a quiescent $V_{DS,Q} = 110 \text{ V}$ resulted in $G_T = 7.5 \text{ dB}$ and $P_{\text{out}} = 43 \text{ dBm}$ (20 W/mm) at a peak PAE of 46.8% [Figure 4(b)]. Figure 4(c) benchmarks the

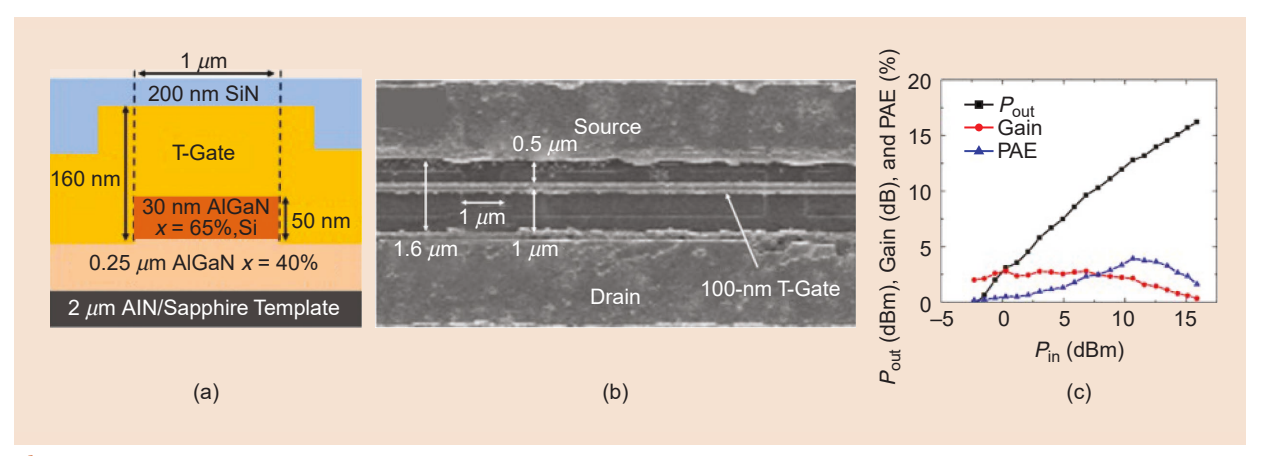


Figure 3. (a) An Al_{0.4}Ga_{0.6}N-channel HEMT using the microchannel structure to reduce the impact of access resistance. (b) A scanning electron microscope image providing a top-side view of the microchannel device. (c) Large-signal measurements of the AlGaN microchannel HEMT with $P_{out} = 2.7$ W/mm at 10 GHz. (Source: [27]; used with permission.)

performance of the GaN-on-AlN HEMT against conventional GaN HEMTs realized on Si or SiC substrates.

A confounding factor in the high-power performance reported for the aforementioned GaN-on-AlN HEMT [37] is the use of an improved deposition strategy for SiN surface passivation. The authors reported an $E_{\rm B}$ of ~6 MV/cm when using low-pressure chemical vapor deposition (LPCVD) SiN versus ~3 MV/cm for PECVD SiN, as shown in Figure 5(a) and consequently claim that this increases the HEMT's overall $V_{\rm BR}$. It is, thus, necessary to understand whether the AlN substrate [with UWBG Al(Ga)N buffer layers] or the enhanced SiN drive performance. In another report

of GaN-on-AlN HEMTs [38], it was demonstrated that higher breakdown voltages can be achieved with AlN substrates versus SiC substrates [Figure 5(b)]. The authors attributed this result to improved thin film quality on AlN versus SiC due to the smaller lattice constant mismatch presented by AlN. A similar result was independently observed by another group when comparing carbon-doped GaN buffer layers versus undoped AlN buffer layers.

As shown in Figure 5(c), the $V_{\rm BR}$ scaling for GaN HEMTs made on a UWBG AlN buffer layers was 140 V/ μ m, which represented an improvement over 100–120-V/ μ m $V_{\rm BR}$ scaling observed in devices grown

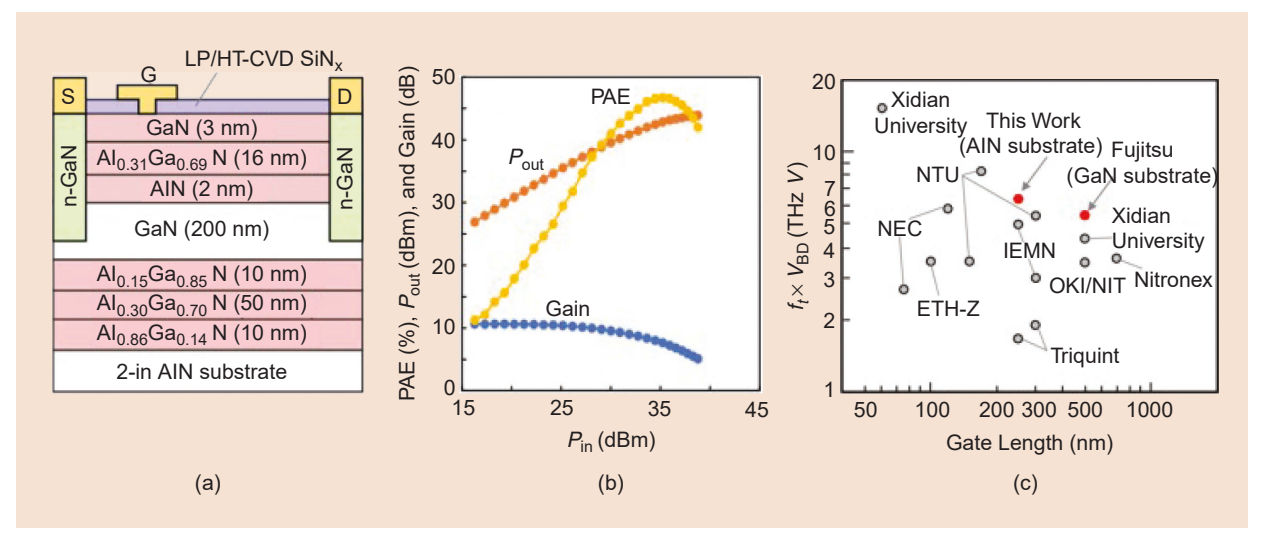


Figure 4. (a) A cross section of a GaN-channel HEMT realized on bulk AlN substrate. (b) Large-signal measurements of the GaN-on-AlN HEMT with P_{out} of >20 W/mm at 8 GHz. (c) A comparison of $f_t \times V_{BR}$ (V_{BD}) as a function of the gate length (L_G). The gray data points were realized on conventional Si or SiC substrates. S: source; G: gate; D: drain; LP/HT-CVD: low-pressure/high temperature chemical-vapor-deposition. (Source: [37]; used with permission.)

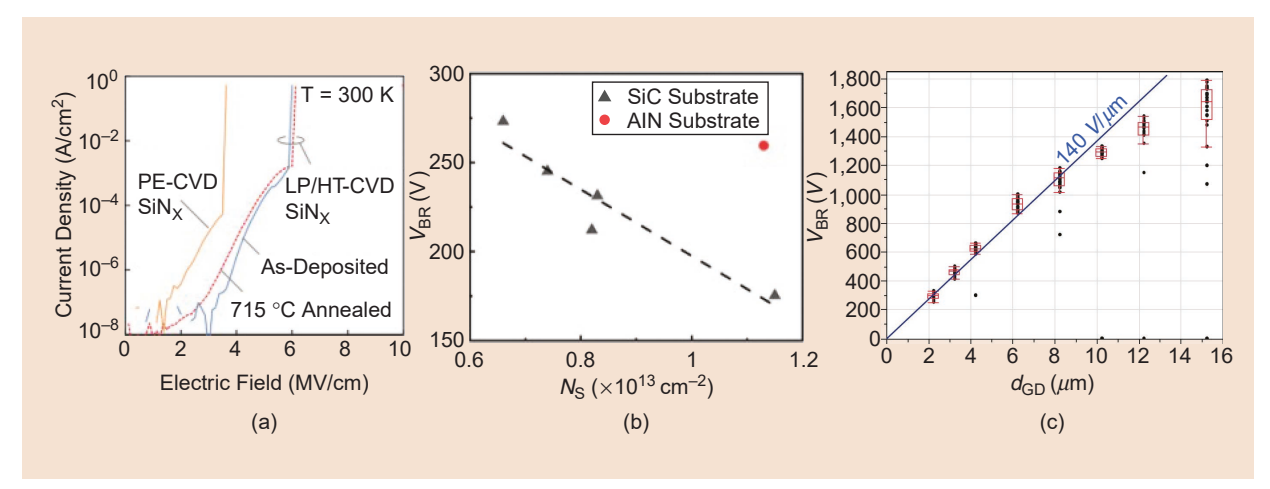


Figure 5. (a) The breakdown limits of SiN passivation layers deposited on AlGaN/GaN HEMTs via PECVD and LPCVD. The use of LPCVD increases E_B. (Source: [37]; used with permission.) (b) and (c) The breakdown voltage (V_{BR}) of AlGAN/GaN HEMTs on (b) AlN substrates (Source: adapted from [38]; used with permission) and (c) thick AlN buffer layers (Source: [39]; used with permission). PE-CVD: plasma-enhanced chemical vapor deposition.

on GaN buffer layers [39]. Moreover, the use of undoped buffer layers reduced trapping effects that cause current collapse and reduce P_{out} . These results suggest that "wrapping" the GaN channel with UWBG Al(Ga)N can increase E_B significantly [40]. In conflict with these results, however, a very recent study achieved $P_{\text{out}} = 31 \text{ W/mm}$ at the X band in InAlN/ GaN HEMTs on SiC substrates [41]. The authors once again highlighted the importance of high-temperature SiN deposition for improved breakdown voltage and reduced access resistance, i.e., high μ and N_S . These results underline the complexity of optimizing IIInitride HEMTs. The design space is further expanded when considering solutions for thermal management with diamond passivation and/or substrates [19], [42]. Nonetheless, it is clear that more performance can be extracted from GaN HEMTs by integrating materials with high E_B (e.g., UWBG III-nitrides) and further improving dielectric/semiconductor interfaces. As these avenues are pursued, the performance will need to be carefully benchmarked against HEMTs with UWBG channels.

These discussed studies were all implemented using metal-polar crystal orientations. However, the high performance of N-polar GaN HEMTs [3] has also inspired the development of UWBG N-polar devices, where the benefits of gate scaling, contact resistance, and a natural back barrier remain relevant. Once again, studies using AlGaN [43, [44], [45] and GaN channels [46] have both emerged. In the latter case, shown in Figure 6, N-polar GaN/AlGaN/AlN HEMTs were realized on bulk AlN substrates [46]. Using $L_{\rm G}=60$ nm, $f_{\rm T}/f_{\rm MAX}$ of 68/100 GHz were achieved, which is promising. Breakdown and large-signal measurements are forthcoming, which will be key to confirming hopes that these structures offer superior E-field and thermal management.

Ga_2O_3

The ability to manufacture high-quality substrates at scale using melt growth techniques combined with its inherently large E_C has made Ga₂O₃ a compelling competitor to UWBG III-nitrides. In one of the first RF device reports, a $Ga_2O_3MOSFET$ with L_G/L_{GD} of 0.7/1.6 μ m was fabricated, achieving f_T/f_{MAX} of 3/11 GHz for $V_{DS} = 25 \text{ V}$ [47]. At 800 MHz, P_{SAT} was 13.7 dBm, corresponding to 0.23 W/mm. Since then, advances in epitaxial growth and doping have made it possible to improve channel mobility as well as $R_{\rm C}$. Using a 60-nm thin channel, degenerately doped (n++)-source/drain (regions and an atomic layer disposition (ALD) SiO2 gate oxide, the channel's R_{SH} and μ were measured to be 14.2 k Ω/\Box and 80 cm 2 /Vs, respectively [48]. While R_C to the metalorganic chemical vapor deposition-based contact layers was extremely low at 0.078 Ω·mm, the FET's total resistance (R_{ON}) suffered from a high interface resistance ($R_{\rm INT}$). Using $L_{\rm G}/L_{\rm GD}$ of 175 nm/0.355 μ m, $f_{\rm T}/f_{\rm MAX}$ of 11/48 GHz and $V_{\rm BR}$ of 192 V ($E_{\rm B}$ of 5.4 MV/cm) were obtained, corresponding to a JFOM of 2.1 THz-V, with results depicted in Figure 7. In unpublished work from the same authors, it has been claimed that, by reducing the large R_{INT} , a JFOM of 3.4 THz-V has been obtained [49].

Using a unique approach, Ga_2O_3 MOSFETs with $N_S = 3.2 \times 10^{13}$ cm⁻² and $\mu = 23$ cm²/Vs were obtained with shallow Si implantation followed by RTA [50]. Using $L_G = 0.15~\mu$ m, the resulting $f_T/f_{\rm MAX}$ of 29/35 GHz and $V_{\rm BR}$ of 193 V correspond to a JFOM of 5.6 THz-V, which is certainly competitive with GaN technology. Large-signal measurements at $V_{\rm DS} = 10$ V were, however, performed on devices with $L_G = 0.5~\mu$ m and achieved a maximum output power of 11.2 dBm (65 mW/mm). More studies are needed to understand if this approach can be used effectively, in particular

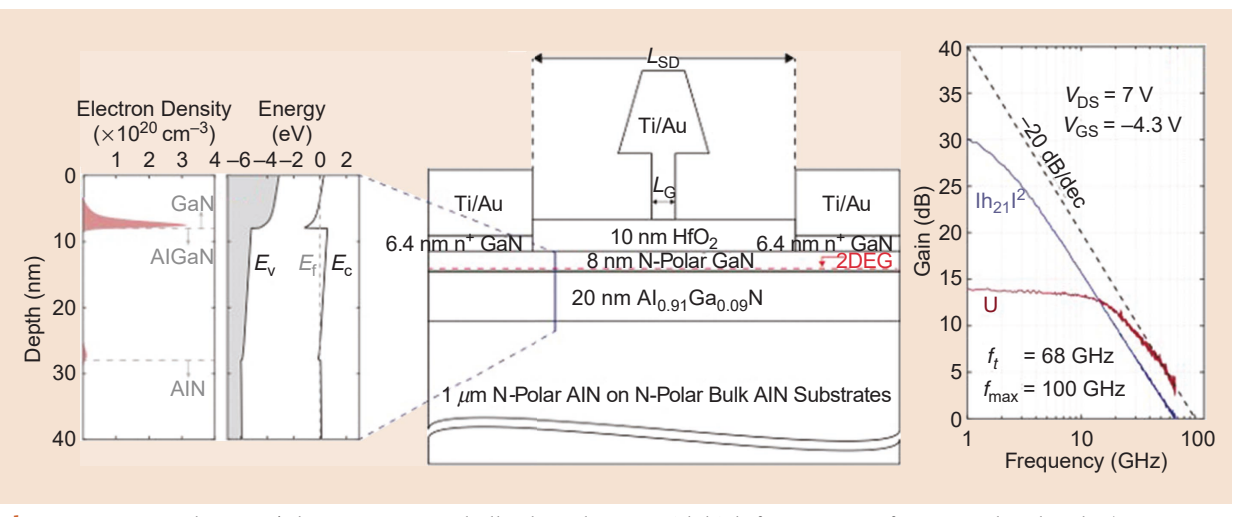


Figure 6. An N-polar GaN/AlGaN HEMT on bulk AlN substrate with high-frequency performance. dec: decade. (Source: [46]; used with the permission of AIP Publishing.)

to overcome incomplete ionization with postimplantation annealing. In a bid to improve thermal dissipation, the same group also transferred Ga_2O_3 to SiC substrates [51]. This unlocked a 2–3× improvement in $I_{\rm MAX}$, which also permitted $P_{\rm out}$ to increase to 296 mW/mm. Heterogeneous integration of Ga_2O_3 and SiC for superior thermal management represents a highly active research topic at this time [52], [53]. Package-level solutions to the same problem are also being developed [54].

 $\beta(Al_xGa_{1-x})_2O_3/Ga_2O_3$ ("AlGo/Go") heterojunction transistors have also been developed in an effort to improve performance at high frequency. Since polarization effects are not present in this material system, modulation doping is required to produce a 2DEG. Temperature-dependent Hall measurements of such an MBE-grown heterojunction unveiled channel mobilities of 143 cm²/Vs and 1,520 cm²/Vs at room temperature (RT) and 50 K, respectively [55]. Measurements of twoterminal constricted channel structures at 50 K allowed v_s to be estimated as 1.1×10^7 cm/s, which is comparable to GaN. Reflecting the mobility's large temperature dependence, MODFETs with $L_{\rm G}/L_{\rm GD}$ of 0.91/0.38 $\mu{\rm m}$ were also measured at RT and 50 K, resulting in f_T/f_{MAX} of 3/17.6 GHz and 12.2/52.3 GHz, respectively. At RT, a $V_{\rm BR}$ of 122.4 V was measured, corresponding to an $E_{\rm B}$ of 3.22 MV/cm. Assuming V_{BD} is temperature insensitive, effective JFOMs for these devices are 0.37 and 1.49 THz-V at RT and 50 K, respectively.

In more recent work, Schottky-gated Ga₂O₃ MOD-FETs with aggressively scaled source access regions were fabricated to overcome the low mobility [56], leading to $f_{\rm T}/f_{\rm MAX}$ of 30/37 GHz and $V_{\rm BR}$ of 23 V. The resulting JFOM is ~0.7 THz-V, which is not only inferior to GaN but also to Ga₂O₃ MOSFETs. This is attributed to the low $N_{\rm S}$ of approximately 2 × 10¹² cm⁻², which is about 10× smaller than what is achievable in GaN HEMTs. To address this, theoretical studies of AlN/ β Ga₂O₃ HEMTs have been carried out [57], [58], but serious challenges relating to epitaxy remain to realize these structures experimentally.

Diamond

As noted in Table 1, diamond provides a compelling mixture of electrical and thermal properties—in this sense, it has often been referred to as the "ideal" semiconductor. The most common strategy for channel formation is to subject the surface to a hydrogen plasma, in turn terminating the surface with H and inducing a quasi-2D hole gas. In an early demonstration 20 years ago, single-crystal homoepitaxial films were grown on 3 × 3-mm² singlecrystal substrates, exhibiting a channel of μ_p of 150 cm²/ Vs and $N_{\rm S}$ of 5 × 10¹² cm⁻², resulting in $R_{\rm SH}$ of 8.3 k Ω/\Box [59]. While this value is larger than the typical R_{SH} obtainable in GaN- and AlGaN-channel devices, it is quite comparable to Ga₂O₃ technology. Alloyed Au contacts were used for ohmics at the S/D, while Al was used as a Schottky gate. Interestingly, while the authors observed a slight V_{TH} shift in their devices over a six-month period of storage in ambient conditions, the resistance of the device remained largely unchanged. This indicates that, under ambient conditions, the H termination can be maintained

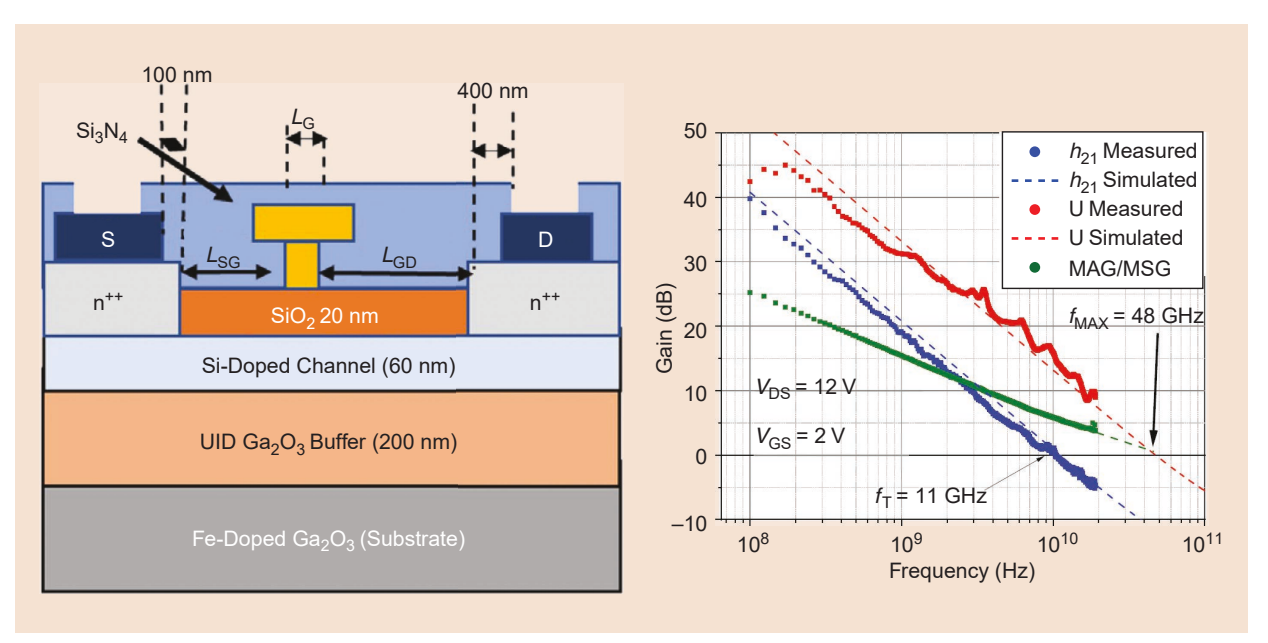


Figure 7. A Ga_2O_3 MOSFET with regrown S/D contacts and record high-frequency performance. UID: unintentionally doped; U: unilateral gain; MAG: maximum available gain; MSG: maximum stable gain. (Source: [48]; used with the permission of AIP Publishing.)

over an extended period. Using L_G of 0.9 μ m, f_T/f_{MAX} values of 24.6/80 GHz were obtained.

With time, larger area ($10 \times 10 \text{ mm}^2$) polycrystalline substrates became commercially available, exhibiting grain sizes of $100 \, \mu\text{m}$ —large enough to fit a highly scaled RF device [60]. Indeed, by reducing the source access resistance ($L_{\text{SG}} = 0.5 \, \mu\text{m}$) and moving to an L_{G} of $100 \, \text{nm}$, I_{MAX} increased to $550 \, \text{mA/mm}$, and $f_{\text{T}}/f_{\text{MAX}}$ reached $38/120 \, \text{GHz}$. This exceeds the high-speed transistor limits seen in Ga_2O_3 technology thus far.

Concerns over the long-term stability of the H termination has driven interest in surface passivation, notably using transition metal oxides, such as V₂O₅ and MoO₃ [61], [62] as well as high-k dielectrics, such as Al₂O₃ and HfO₂ introduced via ALD [63], [64]. Diamond MOSFETs with P_{out} of >1 W/mm up to 2 GHz have, thus, been achieved [65], [66], [67], [68]. The highest reported *P*_{out} is 4.2 W/mm at 2 GHz [69], as shown in Figure 8. However, this resulted in f_T and f_{MAX} penalties, with reported values of 6.2 and 17 GHz, respectively. Recently, highly doped (p++) regrown contacts have also been reported, but R_{INT} remains a challenge [66]. Finally, it should be mentioned that c-BN/diamond heterostructures have been predicted to provide the ultimate path toward high-power diamond-channel transistors [70], representing a shift away from H-terminated strategies. c-BN promises to provide not only high $E_{\rm C}$ but high $\kappa_{\rm th}$ too, making it highly attractive. The challenge is that the cubic phase of BN is thermodynamically unfavorable. Recently, however, ion beam-assisted MBE has produced epitaxial c-BN-on-diamond films with >99% phase purity [21]. If this process can be harnessed at scale, it could represent a major shift in the prospects of diamond technology.

What About Vertical Transistors?

Examples of high-frequency vertical transistors implemented with UWBGSs are rare.

Conventionally, for example, a vertical topology is adopted for HBTs with n-p-n or p-n-p configurations. Besides diamond, however, hole mobility in UWBGSs is very low. Moreover, both doping efficiency and R_C are major challenges to achieving practical amplification. To address this, researchers are investigating methods for heterogeneous integration at the material level, for example, using GaAs/diamond junctions at the base-collector junction of HBTs [71]. Interface trap density and leakage current remain challenges, but, if

Examples of high-frequency vertical transistors implemented with UWBGSs are rare.

overcome, this approach would open the door to an expansive device design space.

Summary

The allure of tapping into the larger E_C of UWBGSs has driven ever-growing interest in these materials for high-performance devices. Al(Ga)N, Ga₂O₃, and diamond represent the three most developed technologies, with each possessing varying degrees of technological maturity and performance strengths. Al(Ga)N represents the most advanced case and directly builds off the industry's deep experience with and knowledge of GaN technology. Ga₂O₃ benefits from low-cost native substrates, but low mobilities and sheet charge densities challenge performance. Diamond continues to intrigue the community, but it remains prohibitively expensive for commercial applications, and H-terminated channels have yet to outperform GaN. In all cases, performance has yet to fulfill the potential predicted by the aforementioned FOMs. However, niche applications, such as high-temperature environments, may provide a foothold for commercialization. Moreover, novel solutions may be found via codesign strategies that incorporate both electronic and thermal considerations at the materials level.

Acknowledgment

Spyridon Pavlidis acknowledges partial support from the National Science Foundation CAREER Award (ECCS-2145340). Greg Medwig and Michael Thomas

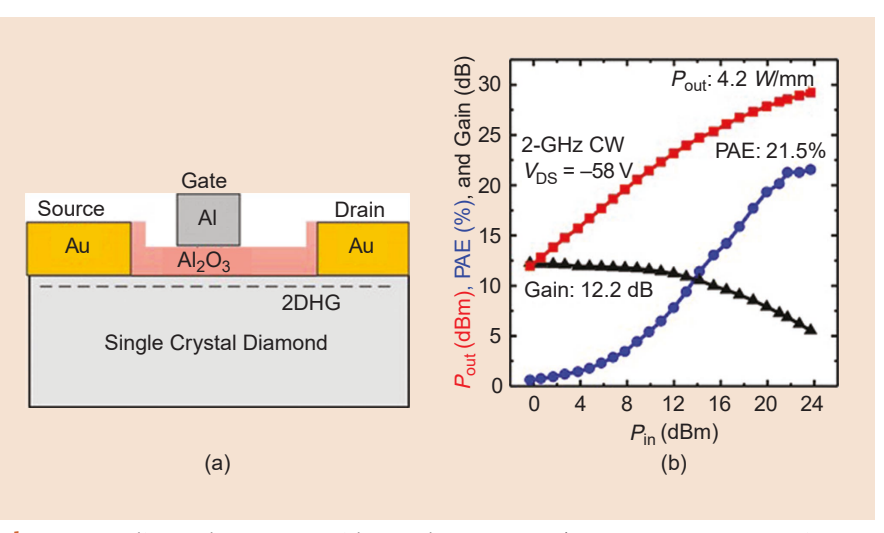


Figure 8. A diamond MOSFET with record $P_{out} = 4.2$ W/mm at 2 GHz. CW: continuous wave; 2DHG: two-dimensional hole gas. (Source: [69]; used with permission).

were supported by the Provost Doctoral Fellowship at North Carolina State University. Spyridon Pavlidis thanks Dr. Guillaume Callet for his encouragement in preparing this article. Greg Medwig and Michael Thomas contributed equally to this work.

References

- Y. Wu, M. Moore, A. Saxler, T. Wisleder, and P. Parikh, "40-W/mm double field-plated GaN HEMTs," in *Proc. 64th Device Res. Conf.*, Jun. 2006, pp. 151–152, doi: 10.1109/DRC.2006.305162.
- [2] Y. Tang et al., "Ultrahigh-speed GaN high-electron-mobility transistors with f_T/f_{max} of 454/444 GHz," IEEE Electron Device Lett., vol. 36, no. 6, pp. 549–551, Jun. 2015, doi: 10.1109/LED.2015.2421311.
- [3] B. Romanczyk et al., "Demonstration of constant 8 W/mm power density at 10, 30, and 94 GHz in state-of-the-art millimeter-wave N-polar GaN MISHEMTS," *IEEE Trans. Electron Devices*, vol. 65, no. 1, pp. 45–50, Jan. 2018, doi: 10.1109/TED.2017.2770087.
- [4] T. P. Nidhi, A. Chakraborty, S. Keller, and U. K. Mishra, "Study of impact of access resistance on high-frequency performance of AlGaN/GaN HEMTs by measurements at low temperatures," *IEEE Electron Device Lett.*, vol. 27, no. 11, pp. 877–880, Nov. 2006, doi: 10.1109/LED.2006.884720.
- [5] T. Palacios et al., "Influence of the dynamic access resistance in the g/sub m/and f/sub T/linearity of AlGaN/GaN HEMTs," *IEEE Trans. Electron Devices*, vol. 52, no. 10, pp. 2117–2123, Oct. 2005, doi: 10.1109/TED.2005.856180.
- [6] M. W. Rahman, N. K. Kalarickal, H. Lee, T. Razzak, and S. Rajan, "Integration of high permittivity BaTiO₃ with AlGaN/GaN for neartheoretical breakdown field kV-class transistors," *Appl. Phys. Lett.*, vol. 119, no. 19, Nov. 2021, Art. no. 193501, doi: 10.1063/5.0070665.
- [7] T. Feng, H. Zhou, Z. Cheng, L. S. Larkin, and M. R. Neupane, "A critical review of thermal boundary conductance across wide and ultrawide bandgap semiconductor interfaces," ACS Appl. Mater. Interfaces, vol. 15, no. 25, pp. 29,655–29,673, Jun. 2023, doi: 10.1021/acsami.3c02507.
- [8] J. Y. Tsao et al., "Ultrawide-bandgap semiconductors: Research opportunities and challenges," Adv. Electron. Mater., vol. 4, no. 1, 2018, Art. no. 1600501, doi: 10.1002/aelm.201600501.
- [9] N. Donato, N. Rouger, J. Pernot, G. Longobardi, and F. Udrea, "Diamond power devices: State of the art, modelling, figures of merit and future perspective," J. Phys. D Appl. Phys., vol. 53, no. 9, Dec. 2019, Art. no. 093001, doi: 10.1088/1361-6463/ab4eab.
- [10] T. P. Chow, I. Omura, M. Higashiwaki, H. Kawarada, and V. Pala, "Smart power devices and ICs using GaAs and wide and extreme bandgap semiconductors," *IEEE Trans. Electron Devices*, vol. 64, no. 3, pp. 856–873, Mar. 2017, doi: 10.1109/TED.2017.2653759.
- [11] P. J. Gielisse et al., "Lattice infrared spectra of boron nitride and boron monophosphide," *Phys. Rev.*, vol. 155, no. 3, pp. 1039–1046, Mar. 1967, doi: 10.1103/PhysRev.155.1039.
- [12] L. Lindsay, D. A. Broido, and T. L. Reinecke, "First-principles determination of ultrahigh thermal conductivity of boron arsenide: A competitor for diamond?" *Phys. Rev. Lett.*, vol. 111, no. 2, Jul. 2013, Art. no. 025901, doi: 10.1103/PhysRevLett.111.025901.
- [13] R. Quay, C. Moglestue, V. Palankovski, and S. Selberherr, "A temperature dependent model for the saturation velocity in semiconductor materials," *Mater. Sci. Semicond. Process.*, vol. 3, nos. 1–2, pp. 149–155, Mar. 2000, doi: 10.1016/S1369-8001(00)00015-9.
- [14] K. Ghosh and U. Singisetti, "Ab initio velocity-field curves in monoclinic β -Ga₂O₃," *J. Appl. Phys.*, vol. 122, no. 3, Jul. 2017, Art. no. 035702, doi: 10.1063/1.4986174.
- [15] M. Zhu, M. Matsubara, and E. Bellotti, "Carrier transport in cubic boron nitride: First-principles and semiempirical models," *Phys. Rev. Appl.*, vol. 20, no. 3, Sep. 2023, Art. no. 034055, doi: 10.1103/ PhysRevApplied.20.034055.
- [16] M. Sotoodeh, A. H. Khalid, and A. A. Rezazadeh, "Empirical low-field mobility model for III–V compounds applicable in device simulation codes," J. Appl. Phys., vol. 87, no. 6, pp. 2890–2900, Mar. 2000, doi: 10.1063/1.372274.

- [17] L. A. M. Lyle, "Critical review of Ohmic and Schottky contacts to β -Ga₂O₃," *J. Vac. Sci. Technol. A*, vol. 40, no. 6, Nov. 2022, Art. no. 060802, doi: 10.1116/6.0002144.
- [18] M. E. Coltrin, A. G. Baca, and R. J. Kaplar, "Analysis of 2D transport and performance characteristics for lateral power devices based on AlGaN alloys," ECS J. Solid State Sci. Technol, vol. 6, no. 11, Oct. 2017, Art. no. S3114, doi: 10.1149/2.0241711jss.
- [19] M. Malakoutian et al., "Low thermal budget growth of near-iso-tropic diamond grains for heat spreading in semiconductor devices," Adv. Functional Mater., vol. 32, no. 47, 2022, Art. no. 2208997, doi: 10.1002/adfm.202208997.
- [20] O. Ueda, M. Kasu, and H. Yamaguchi, "Structural characterization of defects in EFG- and HVPE-grown β-Ga₂O₃ crystals," *Jpn. J. Appl. Phys.*, vol. 61, no. 5, Apr. 2022, Art. no. 050101, doi: 10.35848/1347-4065/ac4b6b.
- [21] D. F. Storm et al., "Mg-facilitated growth of cubic boron nitride by ion beam-assisted molecular beam epitaxy," *Phys. Status Solidi* (*RRL*) – *Rapid Res. Lett.*, vol. 16, no. 7, 2022, Art. no. 2200036, doi: 10.1002/pssr.202200036.
- [22] K. Hussain et al., "High figure of merit extreme bandgap A_{10.87}Ga_{0.13}N-A_{10.64}Ga_{0.36}N heterostructures over bulk AlN substrates," Appl. Phys. Express, vol. 16, Jan. 2023, Art. no. 014005, doi: 10.35848/1882-0786/acb487.
- [23] D. Khachariya et al., "Record >10 MV/cm mesa breakdown fields in A_{10.85}Ga_{0.15}N/A_{10.6}Ga_{0.4}N high electron mobility transistors on native AlN substrates," Appl. Phys. Lett., vol. 120, no. 17, Apr. 2022, Art. no. 172106, doi: 10.1063/5.0083966.
- [24] A. G. Baca et al., "A_{10.85}Ga_{0.15}N/A_{10.70}Ga_{0.30}N high electron mobility transistors with Schottky gates and large on/off current ratio over temperature," ECS J. Solid State Sci. Technol., vol. 6, no. 12, pp. Q161– Q165, 2017, doi: 10.1149/2.0231712jss.
- [25] H. Xue et al., "A_{10.75}Ga_{0.25}N/A_{10.6}Ga_{0.4}N heterojunction field effect transistor with f_T of 40 GHz," Appl. Phys. Express, vol. 12, no. 6, May 2019, Art. no. 066502, doi: 10.7567/1882-0786/ab1cf9.
- [26] H. Xue et al., "All MOCVD grown A_{10.7}Ga_{0.3}N/A_{10.5}Ga_{0.5}N HFET: An approach to make ohmic contacts to Al-rich AlGaN channel transistors," Solid-State Electron., vol. 164, Feb. 2020, Art. no. 107696, doi: 10.1016/j.sse.2019.107696.
- [27] H. Xue et al., "A_{10.65}Ga_{0.35}N/A_{10.4}Ga_{0.6}N micro-channel heterojunction field effect transistors with current density over 900 mA/mm," *IEEE Electron Device Lett.*, vol. 41, no. 5, pp. 677–680, May 2020, doi: 10.1109/LED.2020.2977997.
- [28] S. H. Sohel et al., "X-band power and linearity performance of compositionally graded AlGaN channel transistors," *IEEE Electron Device Lett.*, vol. 39, no. 12, pp. 1884–1887, Dec. 2018, doi: 10.1109/ LED.2018.2874443.
- [29] H. Ye, M. Gaevski, G. Simin, A. Khan, and P. Fay, "Electron mobility and velocity in A_{10.45}Ga_{0.55}N-channel ultra-wide bandgap HEMTs at high temperatures for RF power applications," *Appl. Phys. Lett.*, vol. 120, no. 10, Mar. 2022, Art. no. 103505, doi: 10.1063/5.0084022.
- [30] B. A. Klein et al., "Saturation velocity measurement of A_{10.7}Ga_{0.3}N-channel high electron mobility transistors," *J. Electron. Mater.*, vol. 48, no. 9, pp. 5581–5585, Sep. 2019, doi: 10.1007/s11664-019-07421-1.
- [31] M. Farahmand et al., "Monte Carlo simulation of electron transport in the III-nitride wurtzite phase materials system: Binaries and ternaries," *IEEE Trans. Electron Devices*, vol. 48, no. 3, pp. 535–542, Mar. 2001, doi: 10.1109/16.906448.
- [32] A. F. M. Anwar, S. Wu, and R. T. Webster, "Temperature dependent transport properties in GaN, Al/sub x/Ga/sub 1-x/N, and In/sub x/Ga/sub 1-x/N semiconductors," *IEEE Trans. Electron Devices*, vol. 48, no. 3, pp. 567–572, Mar. 2001, doi: 10.1109/16.906452.
- [33] N. Yafune, S. Hashimoto, K. Akita, Y. Yamamoto, H. Tokuda, and M. Kuzuhara, "AlN/AlGaN HEMTs on AlN substrate for stable high-temperature operation," *Electron. Lett.*, vol. 50, no. 3, pp. 211– 212, 2014, doi: 10.1049/el.2013.2846.
- [34] M. Hiroki, Y. Taniyasu, and K. Kumakura, "High-temperature performance of AlN MESFETs with epitaxially grown n-type AlN channel layers," *IEEE Electron Device Lett.*, vol. 43, no. 3, pp. 350– 353, Mar. 2022, doi: 10.1109/LED.2022.3141100.

- [35] A. Hickman et al., "First RF power operation of AlN/GaN/AlN HEMTs with >3 A/mm and 3 W/mm at 10 GHz," IEEE J. Electron Devices Soc., vol. 9, pp. 121–124, 2021, doi: 10.1109/JEDS.2020.3042050.
- [36] A. Hickman et al., "High breakdown voltage in RF AlN/GaN/AlN quantum well HEMTs," IEEE Electron Device Lett., vol. 40, no. 8, pp. 1293–1296, Aug. 2019, doi: 10.1109/LED.2019.2923085.
- [37] J. Kotani et al., "24.4 W/mm X-band GaN HEMTs on AlN substrates with the LPCVD-grown high-breakdown-field SiNx layer," IEEE J. Electron Devices Soc., vol. 11, pp. 101–106, 2023, doi: 10.1109/ JEDS.2023.3234235.
- [38] S. Ozaki et al., "First demonstration of X-band AlGaN/GaN high electron mobility transistors using free-standing AlN substrate over 15 W mm-1 output power density," Appl. Phys. Express, vol. 14, no. 4, Mar. 2021, Art. no. 041004, doi: 10.35848/1882-0786/abec90.
- [39] O. Hilt et al., "10 A/950 V switching of GaN-channel HFETs with non-doped AlN buffer," in *Proc. 35th Int. Symp. Power Semicond. Devices ICs (ISPSD)*, Hong Kong, May 2023, pp. 374–377, doi: 10.1109/ISPSD57135.2023.10147681.
- [40] J. Bassaler, R. Comyn, C. Bougerol, Y. Cordier, F. Medjdoub, and P. Ferrandis, "Transport properties of a thin GaN channel formed in an Al_{0.9}Ga_{0.1}N/GaN heterostructure grown on AlN/sapphire template," J. Appl. Phys., vol. 131, no. 12, Mar. 2022, Art. no. 124501, doi: 10.1063/5.0077107.
- [41] A. Yamada et al., "31 W/mm at 8 GHz in InAlGaN/GaN HEMT with thermal CVD SiN_x passivation," IEEE Electron Device Lett., vol. 45, no. 3, pp. 324–327, Mar. 2024, doi: 10.1109/LED.2024.3355051.
- [42] W. S. Lee, K. Won Lee, S. H. Lee, K. Cho, and S. Cho, "A GaN/diamond HEMTs with 23 W/mm for next generation high power RF application," in *Proc. IEEE MTT-S Int. Microw. Symp.* (IMS), Boston, MA, USA, Jun. 2019, pp. 1395–1398, doi: 10.1109/MWSYM.2019.8700882.
- [43] J. Lemettinen, N. Chowdhury, H. Okumura, I. Kim, S. Suihkonen, and T. Palacios, "Nitrogen-polar polarization-doped field-effect transistor based on A_{10.8}Ga_{0.2}N/AlN on SiC with drain current over 100 mA/mm," *IEEE Electron Device Lett.*, vol. 40, no. 8, pp. 1245– 1248, Aug. 2019, doi: 10.1109/LED.2019.2923902.
- [44] D. Inahara et al., "Investigation of electrical properties of N-polar AlGaN/AlN heterostructure field-effect transistors," *Phys. Status Solidi A*, vol. 220, no. 16, 2023, Art. no. 2200871, doi: 10.1002/pssa.202200871.
- [45] Z. Zhang et al., "Polarization-induced 2D electron gases in N-polar AlGaN/AlN heterostructures on single-crystal AlN substrates," Appl. Phys. Lett., vol. 122, no. 21, May 2023, Art. no. 212106, doi: 10.1063/5.0145826.
- [46] E. Kim et al., "N-polar GaN/AlGaN/AlN high electron mobility transistors on single-crystal bulk AlN substrates," Appl. Phys. Lett., vol. 122, no. 9, Feb. 2023, Art. no. 092104, doi: 10.1063/5.0138939.
- [47] A. J. Green et al., β-Ga₂O₃ MOSFETs for radio frequency operation," IEEE Electron Device Lett., vol. 38, no. 6, pp. 790–793, Jun. 2017, doi: 10.1109/LED.2017.2694805.
- [48] C. N. Saha et al., "Scaled β -Ga₂O₃ thin channel MOSFET with 5.4 MV/cm average breakdown field and near 50 GHz f_{MAX}," *Appl. Phys. Lett.*, vol. 122, no. 18, May 2023, Art. no. 182106, doi: 10.1063/5.0149062.
- [49] C. N. Saha, A. Vaidya, A. F. M. A. U. Bhuiyan, L. Meng, H. Zhao, and U. Singisetti, "Sub-100 nm β -Ga₂O₃ MOSFET with 55 GHz f_{MAX} and >100 V breakdown," 2023, [Online]. Available: https://doi-org.prox.lib.ncsu.edu/10.1063/5.0208580
- [50] X. Yu et al., "High-voltage β -Ga₂O₃ RF MOSFETs with a shallow-ly-implanted 2DEG-like channel," *IEEE Electron Device Lett.*, vol. 44, no. 7, pp. 1060–1063, Jul. 2023, doi: 10.1109/LED.2023.3282454.
- [51] X. Yu et al., "Heterointegrated Ga₂O₃-on-SiC RF MOSFETs with f_T/f_{max} of 47/51 GHz by ion-cutting process," *IEEE Electron Device Lett.*, vol. 44, no. 12, pp. 1951–1954, Dec. 2023, doi: 10.1109/ LED.2023.3327134.
- [52] C.-H. Lin et al., "Single-crystal-Ga₂O₃/polycrystalline-SiC bonded substrate with low thermal and electrical resistances at the heterointerface," *Appl. Phys. Lett.*, vol. 114, no. 3, Jan. 2019, Art. no. 032103, doi: 10.1063/1.5051720.

- [53] Y. Song et al., "Ultra-wide band gap Ga₂O₃-on-SiC MOSFETs," ACS Appl. Mater. Interfaces, vol. 15, no. 5, pp. 7137–7147, Feb. 2023, doi: 10.1021/acsami.2c21048.
- [54] M. Xiao et al., "Packaged Ga₂O₃ Schottky rectifiers with over 60-A surge current capability," *IEEE Trans. Power Electron.*, vol. 36, no. 8, pp. 8565−8569, Aug. 2021, doi: 10.1109/TPEL.2021.3049966.
- [55] Y. Zhang et al., "Evaluation of low-temperature saturation velocity in β -(Al_xGa1-_x)₂O₃/Ga₂O₃ modulation-doped field-effect transistors," *IEEE Trans. Electron Devices*, vol. 66, no. 3, pp. 1574–1578, Mar. 2019, doi: 10.1109/TED.2018.2889573.
- [56] A. Vaidya, C. N. Saha, and U. Singisetti, "Enhancement mode β-(A_{1x}Ga_{1-x})₂O₃/Ga₂O₃ heterostructure FET (HFET) with high transconductance and cutoff frequency," *IEEE Electron Device Lett.*, vol. 42, no. 10, pp. 1444–1447, Oct. 2021, doi: 10.1109/LED.2021. 3104256.
- [57] Y. Lu et al., "AlN/beta-Ga₂O₃ based HEMT: a potential pathway to ultimate high power device," Jan. 2019, *arXiv:1901.05111*.
- [58] K. Song et al., "Normally-off AlN/β-Ga₂O₃ field-effect transistors using polarization-induced doping," J. Phys. D Appl. Phys., vol. 53, no. 34, Jun. 2020, Art. no. 345107, doi: 10.1088/1361-6463/ab8d6e.
- [59] M. Kubovic et al., "Microwave performance evaluation of diamond surface channel FETs," *Diamond Related Mater.*, vol. 13, nos. 4–8, pp. 802–807, Apr. 2004, doi: 10.1016/j.diamond.2003.11.089.
- [60] K. Ueda et al., "Diamond FET using high-quality polycrystalline diamond with f_T of 45 GHz and f_{max} of 120 GHz," IEEE Electron Device Lett., vol. 27, no. 7, pp. 570–572, Jul. 2006, doi: 10.1109/ LED.2006.876325.
- [61] K. G. Crawford et al., "Diamond field-effect transistors with V_2O_5 -induced transfer doping: Scaling to 50-nm gate length," *IEEE Trans. Electron Devices*, vol. 67, no. 6, pp. 2270–2275, Jun. 2020, doi: 10.1109/TED.2020.2989736.
- [62] K. G. Crawford et al., "Thermally stable, high performance transfer doping of diamond using transition metal oxides," Sci Rep., vol. 8, no. 1, Feb. 2018, Art. no. 3342, doi: 10.1038/s41598-018-21579-4.
- [63] A. Daicho, T. Saito, S. Kurihara, A. Hiraiwa, and H. Kawarada, "High-reliability passivation of hydrogen-terminated diamond surface by atomic layer deposition of A_{I2}O₃," J. Appl. Phys., vol. 115, no. 22, Jun. 2014, Art. no. 223711, doi: 10.1063/1.4881524.
- [64] M. W. Geis et al., "Stable, low-resistance, 1.5 to $3.5 \,\mathrm{k\Omega} \,\mathrm{s}^{q-1}$, diamond surface conduction with a mixed metal-oxide protective film," *Diamond Related Mater.*, vol. 106, Jun. 2020, Art. no. 107819, doi: 10.1016/j. diamond.2020.107819.
- [65] X. Yu et al., "1 W/mm output power density for H-terminated diamond MOSFETs with A₁₂O₃/SiO₂ Bi-layer passivation at 2 GHz," *IEEE J. Electron Devices Soc.*, vol. 9, pp. 160–164, 2021, doi: 10.1109/ JEDS.2020.3046603.
- [66] K. Kudara et al., "Over 1 A/mm drain current density and 3.6 W/mm output power density in 2DHG diamond MOSFETs with highly doped regrown source/drain," Carbon, vol. 188, pp. 220–228, Mar. 2022, doi: 10.1016/j.carbon.2021.11.034.
- [67] S. Imanishi et al., "3.8 W/mm RF power density for ALD A₁₂O₃-based two-dimensional hole gas diamond MOSFET operating at saturation velocity," *IEEE Electron Device Lett.*, vol. 40, no. 2, pp. 279–282, Feb. 2019, doi: 10.1109/LED.2018.2886596.
- [68] K. Kudara et al., "High output power density of 2DHG diamond MOSFETs with thick ALD-A₁₂O₃," IEEE Trans. Electron Devices, vol. 68, no. 8, pp. 3942–3949, Aug. 2021, doi: 10.1109/TED.2021. 3086457.
- [69] C. Yu et al., "Hydrogen-terminated diamond MOSFETs on (0 0 1) single crystal diamond with state of the art high RF power density," Functional Diamond, vol. 2, no. 1, pp. 64–70, Dec. 2022, doi: 10.1080/26941112.2022.2082853.
- [70] J. T. Mullen, J. A. Boulton, M. Pan, and K. W. Kim, "Electronic properties of c-BN/diamond heterostructures for high-frequency high-power applications," 2023, arXiv:2310.06955.
- [71] S. J. Cho et al., "Fabrication of AlGaAs/GaAs/diamond heterojunctions for diamond-collector HBTs," AIP Adv., vol. 10, no. 12, Dec. 2020, Art. no. 125226, doi: 10.1063/5.0027864.

NN.